IUPAC Task Group on Atmospheric Chemical Kinetic Data Evaluation
Data Sheet MD7; V.A2.7

This datasheet last evaluated: June 2016; last change in preferred values: June 2016

HONO + mineral oxide (dust) surfaces → products

Experimental data

Parameter	RH	p_{HONO} /mbar	NO yield	NO_2 yield	Substrate	Temp./K	Reference	Technique/ Comments
Uptake coefficients: γ, γ_0								
$\gamma_{0,BET} = (2.3\pm0.8)\times10^{-3}$		1.2×10^{-5}	42±6	60±9	TiO_2	300	El Zein et al., 2012	CWFT-MS (a)
$\gamma_{0,BET} = (1.8\pm0.7)\times10^{-5}$ (RH)$^{-0.63}$	<12.6	-1.2×10^{-4}	42±6	60±9				
$\gamma_{0,BET} = (1.4\pm0.5)\times10^{-5}$ (exp[(1405±110)/T]	0.001		42±6	60±9		275-320		
$\gamma_{0,BET} = (6.5\pm2.0)\times10^{-4}$		2.4×10^{-5}	40±6	60±9	Al_2O_3	300	Romanias et al., 2012	CWFT-MS (b)
$\gamma_{0,BET} = (4.8\pm1.4)\times10^{-6}$ (RH)$^{-0.61}$ (dark)	<10	-1.5×10^{-4}	40±6	60±9		280-300		
$\gamma_{0,BET} = (1.7\pm0.6)\times10^{-5}$ (RH)$^{-0.44}$ (UV, J_{NO2}=0.012 s^{-1})	<35		40±6	60±9		280-300		
$\gamma_{0,BET} = (2.7\pm0.8)\times10^{-4}$		2.4×10^{-5}	40±6	60±9	Fe_2O_3	300	El Zein et al., 2013a	CWFT-MS (c)
$\gamma_{0,BET} = (1.7\pm0.6)\times10^{-6}$ (RH)$^{-0.62}$	<14	-6.2×10^{-4}	40±6	60±9		300		
$\gamma_{0,BET} = (1.6\pm0.5)\times10^{-4}$			40±6	60±9	ATD	300		
$\gamma_{0,BET} = (3.8\pm1.3)\times10^{-6}$ (RH)$^{-0.61}$	<84		40±6	60±9		275		
$\gamma_{0,BET} = (3.9\pm1.2)\times10^{-3}$		1.2×10^{-5}	48±7	52±8	TiO_2	300	El Zein et al., 2013b	CWFT-MS (d)
$\gamma_{0,BET} = (6.9\pm2.2)\times10^{-5}$ (RH)$^{-0.30}$ (UV, J_{NO2}=0.002-0.012 s^{-1})	<60	-2.1×10^{-4}	48±7	52±8				
$\gamma_{0,BET} = (3.0\pm1.5)\times10^{-5}$ (exp[(1390±150)/T]	0.001		48±7	52±8		275-320		
$\gamma_{geom} = (1.1\pm x)\times10^{-4}$ (pH 1)	30	1.0×10^{-5}			kaolinite	296	Donaldson et al., PNAS, 2014	CWFT-CIMS (e)
$\gamma_{geom} = (1.0\pm0.1)\times10^{-5}$ (pH 3)								
$\gamma_{geom} = (7.5\pm0.5)\times10^{-5}$ (pH 7)								
$\gamma_{geom} = (1.3\pm0.1)\times10^{-4}$ (pH 14)								
$\gamma_{geom} = (2.5\pm0.4)\times10^{-4}$	0	1.0×10^{-5}			soil	296	Donaldson et al., ES&T, 2014	CWFT-CIMS (f)
$\gamma_{geom} = (2.8\pm0.6)\times10^{-5}$	30							
$\gamma_{geom} = (2.0\pm0.6)\times10^{-5}$	50							

$\gamma_{geom} = (1.1\pm0.4)\times10^{-5}$	80						
$\gamma_{geom} = (2.5\pm0.5)\times10^{-4}$	0	4.0×10^{-6}					
$\gamma_{geom} = (2.3\pm0.4)\times10^{-4}$	0	2.0×10^{-5}					
$\gamma_{geom} = (2.1\pm0.3)\times10^{-4}$	0	4.7×10^{-5}					
$\gamma_{geom} = (5.1\pm0.6)\times10^{-5}$	30	0.8					
$\gamma_{geom} = (3.4\pm0.3)\times10^{-5}$	30	3.0×10^{-5}					
$\gamma_{geom} = (3.0\pm0.5)\times10^{-5}$	30	6.1×10^{-5}					
$\gamma = (7.7\pm2.9)\times10^{-6}$	0	3.0×10^{-6}		$NaHCO_3$	298	VandenBoer et al., 2015	CWFT-CIMS (g)
$\gamma = (1.1\pm0.4)\times10^{-5}$	50				298		
$\gamma = (1.1\pm0.5)\times10^{-5}$	90-95				298		
$\gamma = (3.3\pm1.0)\times10^{-6}$	0	3.0×10^{-6}		Na_2CO_3	298		
$\gamma = (6.3\pm1.0)\times10^{-6}$	50				298		
$\gamma = (1.3\pm0.5)\times10^{-5}$	90-95				298		

Comments

(a) TiO_2 films of Aeroxide P25 (50 ± 15 m^2 g^{-1} surface area, ~20 nm particle diameter) were formed from a suspension in ethanol, followed by drying and baking at 100-150°C in vacuo. HONO (0.3 – 3) × 10^{12} molecule cm^{-3}) was produced online via the heterogeneous reaction of HCl with $NaNO_2$. NO (10-20% of HONO) was present as contamination from the HONO source. The pressure dependence of the first order loss rate was used to obtain the gas phase diffusion coefficient of HONO in He at 1.3 mbar of D_0 490±50 Torr cm s that was then used to obtain the geometric uptake coefficient. Its linear mass dependent range was used to calculate uptake coeffients based on BET surface area, γ_{BET}, which was independent of the HONO concentration.

(b) Experimental set up as in (a). Films of γ-Al_2O_3 powders (specific BET surface area of (200 ± 40) m^2 g^{-1}) were formed from a suspension in ethanol, followed by drying and baking at (100-150)°C in vacuo. Samples were irradiated at 315-400 nm, with J_{NO2} in the range (0.002-0.012) s^{-1}. HONO (0.6 – 3.5) × 10^{12} molecule cm^{-3} exhibited complex time dependent uptake with a strong initial loss, followed by partial recovery into a quasi-steady state at around 2-3 min, that slowly decreased further. The loss rate at around 3 min was used to obtain the geometric uptake coefficient. Its linear mass dependent range was used to calculate γ_{BET}, which was independent of the HONO concentration. γ_{BET} increased linearly with UV irradiance and was independent of temperature in the range 275-320 K at 0.2% RH. About 10^{13} molecule cm^{-2} of HONO (of up to 2×10^{14} molecule cm^{-2} of HONO lost to the surface in total after long exposure times) remained unreacted on the surface, as determined via thermal desorption at 250°C, independent of whether the surface was irradiated or not. UV photolysis of unreacted HONO on the surface yielded NO and NO_2 at ratios nearly 3:1 at rates of about 0.1 min^{-1} at J_{NO2} of 0.012 s^{-1}. The authors suggest that the presence of HNO_3 can explain NOx yields from UV photolysis larger than HONO coverages determined by thermal desorption.

(c) Experimental set-up as in (a). Films of Fe_2O_3 and ATD powders (specific BET surface areas of (11 ± 2) m^2 g^{-1} and (85 ± 10) m^2 g^{-1}, respectively) were formed from a suspension in ethanol, followed by drying and baking at (150-170)°C in vacuo. UV irradiation conditions as in (b). HONO concentrations were in the range (0.6 – 15) × 10^{12} molecule cm^{-3}. The linear mass dependent range of the geometric uptake coefficient (at max 0.6 mg/cm) was used to calculate γ_{BET}. γ_{BET} was independent of temperature in the range 275-320 K at 4% (Fe_2O_3) and 5% (ATD) RH. Co-dosing experiments with NO_2 indicated no effect of one of NO_2 or HONO on the uptake of the other.

(d) Experimental set-up as in (a). UV irradiation configuration and conditions as in (b). HONO concentrations were in the range (0 – 5) × 10^{12} molecule cm^{-3}. The linear mass dependent range of the geometric uptake coefficient was used to calculate γ_{BET}, which was independent of the HONO concentration and independent of UV intensity for the range of J_{NO2} (0.002-0.012) s^{-1}. The formation of products NO and NO_2 showed some initial time dependence, ascribed to conversion of NO_2 to NO. 2.8×10^{13} molecule cm^{-2} of HONO remained unreacted on the surface, as determined via thermal desorption at 250°C, independent of initial HONO concentration during previous exposure.

(e) CIMS detection of HONO (10 ppb) using SF_5^- as reagent ion. Kaolinite coatings (0.7 g / 5cm) prepared by applying 1:1 aqueous kaolinite slurries, pH adjusted with H_2SO_4 and NaOH to an 1.7 cm inner diameter Pyrex tube. The geometric uptake coefficient was derived from steady state HONO loss rates and after application of diffusion correction. Experiments were performed in the context of HONO uptake to soil. pH range of minimum uptake coefficient was related to the surface charge assessed with potentiometric measurements.

(f) Setup as in (e). Soil samples collected from Indiana (USA), classified as Genesee, a fine loamy alluvium comprised of silica, aluminosilicates, and less than 3% organic matter were autoclaved and sieved (120 mesh) and an aqueous slurry used to form a surface coating. The geometric uptake coefficient was derived from steady state HONO loss rates as in (e). No correction applied for the BET surface area.

(g) HONO (3 ppb) was produced online via the heterogeneous reaction of HCl with $NaNO_2$. And detected using $CH_3CO_2^-$ ions $NaHCO_3$ and Na_2CO_3 substrates were prepared from 1 mM salt solutions followed by drying at 80 °C to form solid coatings of the surface. Diffusion corrected uptake coefficients reported in the table are based on the geometric surface area HONO uptake was irreversible, no products were observed. HONO release could be observed after exposure to HCl or HNO_3 indicating acid base exchange of HONO with HCO_3^- and CO_3^{2-} in the initial interaction of HONO with these substrates.

Preferred Values

Parameter	**Value**	**T/K**
γ	$(1.6\pm0.5)\times10^{-4}$ $(3.8\pm1.3)\times10^{-6}$ $(RH)^{-0.61}$ (RH<50%)	280-320 280-320
Reliability		
$\Delta\log(\gamma)$	±0.5	280-320

Comments on Preferred Values

The studies providing direct kinetic information for the uptake of HONO to mineral dust and its proxies are from the same group. Since ATD represents the most relevant substrate for atmospheric mineral dusts among those studied, we prefer the values provided by El Zein et al. (2013a), including the humidity dependence, but with a reduced range of RH, justified further below in the discussion of the product yields. Uptake may saturate at long exposure times if HONO accumulates. When compared on the basis of geometric, rather than BET, uptake coefficients, the values reported by Donaldson et al. (2014) for kaolinite and VandenBoer et al. (2015) for Na_2CO_3 and $NaHCO_3$ appear rather low. They were measured under steady state conditions after longer interaction times, while the former represent the uptake coefficient observed during early interaction times as long as surface coverages remain low.

At low humidity and up to 84 % RH for ATD, the initial uptake of HONO on all atmospheric mineral oxides shows a nearly inverse dependence on RH, consistent with water competitively adsorbing to these surfaces.

Uptake on the carbonate salts exhibits opposite behavior due to the progressive dissolution of carbonate and hydrogen carbonate allowing acid-base exchange with HONO to drive uptake.

Formation of NO and NO_2 may proceed through a disproportionation on the surface:

$$HONO_g + HONO_{ads} \rightarrow NO + NO_2 + H_2O \quad \text{(R1)}$$

Reaction R1 may proceed through the formation of N_2O_3 as in aqueous solution.

A second feasible mechanism is via direct redox reaction with surface sites (such as Ti^{3+} or Ti^{4+} on TiO_2):

$$HONO_g + SS \rightarrow NO_2 + NO_2 + H^+ + SS_{red} \quad \text{(R2a)}$$

$$HONO_g + SS_{red} \rightarrow NO_2 + NO_2 + H^+ + SS \quad \text{(R2b)}$$

The combination of R1 and R2 may explain the observed deviation of the yields of NO and NO_2 from 0.5, as pointed out already by Syomin and Finlayson-Pitts (2003), ten Brink and Spoelstra (1998), and Kayser and Wu (1977) based on experiments with Pyrex and borosilicate glass reactor materials. R2 seems not to be relevant for the only authentic dust material studied (ATD, El Zein et al. (2013)), where R1 dominates, with nearly 50% yields.

Since aged atmospheric dusts likely contain soluble coatings, the interaction of HONO may become governed by acid base chemistry modulated by these coatings, their water activity and the ion exchange capacities of the substrates, as demonstrated in the studies by Donaldson et al. (2013a, 2013b) and VandenBoeur et al. (2015). Thus for high relative humidity, kinetics may rather be described by the slower uptake described in these studies. But since they were performed under conditions pertinent to soil uptake extrapolation to atmospheric particles is difficult. We therefore limit the preferred kinetics and product yields to conditions < 50% RH and fresh mineral dust particles.

Uptake of HONO to the pure, proxy mineral oxides listed in the experimental data table exhibits negative temperature dependence, probably indicative of physical adsorption of HONO preceding reaction. The complex mix of minerals in ATD nullifies some of these effects, leading to temperature independent uptake coefficient values and product yields.

The complex mix of materials in ATD may also be the reason why initial uptake and product yields are not sensitive to UV irradiation in the wavelength range of the band gap of some of the photoactive constituents. For the proxy materials studied, UV radiation has an effect for TiO_2 and Al_2O_3, but not so on Fe_2O_3. This suggests that it is not only direct electron-hole pair generation by light in the actinic region (expected for TiO_2 and Fe_2O_3), but also the formation of charge transfer complexes that may allow excitations at sub-bandgap energies, e.g. for Al_2O_3 (Karunakaran et al., 2011).

References

Donaldson, M. A., Berke, A. E., and Raff, J. D.: Environ. Sci. Technol., 48, 375-383, 2013.

Donaldson, M. A., Bish, D. L., and Raff, J. D.: Proc. Natl. Acad. Sci., 111, 18472-18477, 2014.

El Zein, A., Bedjanan, Y. : J. Phys. Chem. A 116, 3665-3672, 2012.

El Zein, A., Bedjanian, Y., and Romanias, M. N.: Atmos. Environ., 67, 203-210, 2013b.

El Zein, A., Romanias, M. N., and Bedjanian, Y.: Environ. Sci. Technol., 47, 6325-6331, 2013a.

Kaiser, E. W., Wu, C. H.: J. Phys. Chem. 81, 1701−1706, 1977.

Karunakaran, C., Dhanalakshmi, R., Manikandan, G., Gomathisankar, P.: Indian J. Chem. 50A, 163–170, 2011.

Romanias, M. N., El Zein, A., and Bedjanian, Y.: J. Photochem. Photobiol. A, 250, 50-57, 2012.

Syomin, D.A., Finlayson-Pitts, B.J.: Phys. Chem. Chem. Phys. 7, 5236-5242, 2003.

Ten Brink, H. M., Spoelstra, H.: Atmos. Environ. 32, 247-251, 1998.

VandenBoer, T. C., Young, C. J., Talukdar, R. K., Markovic, M. Z., Brown, S. S., Roberts, J. M., and Murphy, J. G.: Nature Geosci, 8, 55-60, 2015.

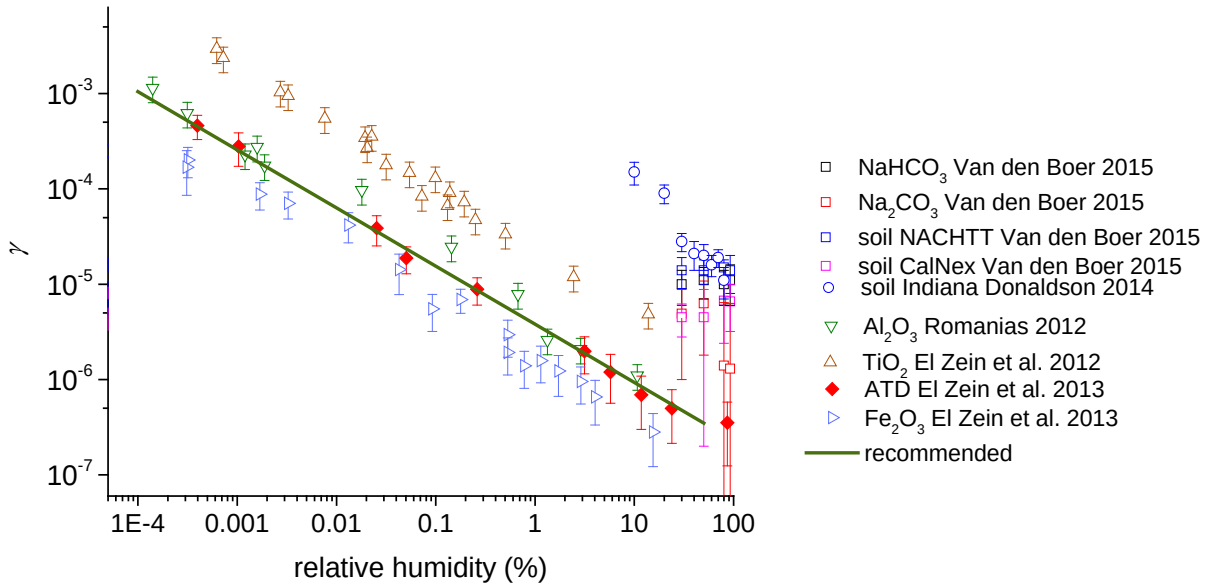

Figure 1: Uptake coefficient of HONO on mineral dust as a function of relative humidity; symbols: experimental data, green line: IUPAC recommendation.